Journal of Neuro-Oncology (2021) 151:267–278
https://doi.org/10.1007/s11060-020-03661-y

CLINICAL STUDY

Quantitative CEST and MT at 1.5T for monitoring treatment response in glioblastoma: early and late tumor progression during chemoradiation

Rachel W. Chan[1] · Hanbo Chen[2] · Sten Myrehaug[2] · Eshetu G. Atenafu[3] · Greg J. Stanisz[1,4,5] · James Stewart[2] · Pejman Jabehdar Maralani[6] · Aimee K. M. Chan[6] · Shadi Daghighi[6] · Mark Ruschin[2] · Sunit Das[7] · James Perry[8] · Gregory J. Czarnota[1,2,4] · Arjun Sahgal[1,2] · Angus Z. Lau[1,4]

Received: 8 September 2020 / Accepted: 7 November 2020 / Published online: 16 November 2020

Abstract

Purpose Quantitative MRI (qMRI) was performed using a 1.5T protocol that includes a novel chemical exchange saturation transfer/magnetization transfer (CEST/MT) approach. The purpose of this prospective study was to determine if qMRI metrics at baseline, at the 10th and 20th fraction during a 30 fraction/6 week standard chemoradiation (CRT) schedule, and at 1 month following treatment could be an early indicator of response for glioblastoma (GBM).

Methods The study included 51 newly diagnosed GBM patients. Four regions-of-interest (ROI) were analyzed: (i) the radiation defined clinical target volume (CTV), (ii) radiation defined gross tumor volume (GTV), (iii) enhancing-tumor regions, and (iv) FLAIR-hyperintense regions. Quantitative CEST, MT, T_1 and T_2 parameters were compared between those patients progressing within 6.9 months (early), and those progressing after CRT (late), using mixed modelling. Exploratory predictive modelling was performed to identify significant predictors of early progression using a multivariable LASSO model.

Results Results were dependent on the specific tumor ROI analyzed and the imaging time point. The baseline CEST asymmetry within the CTV was significantly higher in the early progression cohort. Other significant predictors included the T_2 of the MT pools (for semi-solid at fraction 20 and water at 1 month after CRT), the exchange rate (at fraction 20) and the MGMT methylation status.

Conclusions We observe the potential for multiparametric qMRI, including a novel pulsed CEST/MT approach, to show potential in distinguishing early from late progression GBM cohorts. Ultimately, the goal is to personalize therapeutic decisions and treatment adaptation based on non-invasive imaging-based biomarkers.

Keywords Chemical exchange saturation transfer · Magnetization transfer · Glioblastoma · Treatment monitoring · Radiation oncology

Electronic supplementary material The online version of this article (https://doi.org/10.1007/s11060-020-03661-y) contains supplementary material, which is available to authorized users.

✉ Rachel W. Chan
rchan@sri.utoronto.ca

[1] Physical Sciences, Sunnybrook Research Institute, Toronto, ON, Canada

[2] Department of Radiation Oncology, Sunnybrook Health Sciences Centre, University of Toronto, Toronto, ON, Canada

[3] Department of Biostatistics, University Health Network, University of Toronto, Toronto, ON, Canada

[4] Medical Biophysics, University of Toronto, Toronto, ON, Canada

[5] Department of Neurosurgery and Pediatric Neurosurgery, Medical University, Lublin, Poland

[6] Medical Imaging, Sunnybrook Health Sciences Centre, University of Toronto, Toronto, ON, Canada

[7] Division of Neurosurgery, St Michael's Hospital, University of Toronto, Toronto, ON, Canada

[8] Division of Neurology, Sunnybrook Health Sciences Centre, Toronto, ON, Canada

Introduction

Glioblastoma multiforme (GBM) is the most common and aggressive primary malignant brain tumor [1, 2]. Despite standard treatment which involves surgical resection followed by 6 weeks of chemoradiation (CRT) with concurrent temozolomide chemotherapy and radiation [3], the overall survival (OS) for newly diagnosed GBM patients remains poor with median overall survival rates ranging from 15 to 18 months [1, 2]. Identification of which patients will progress within the 6.9 month median progression-free-survival (PFS) rate, as observed in the practice-defining Stupp [3] randomized trial, remains a challenge with clinical implications for treatment adaptation.

Saturation transfer MRI, including quantitative magnetization transfer (qMT) [4, 5] and chemical exchange saturation transfer (CEST) [6], has been shown to add quantitative MRI (qMRI) based functional information for monitoring response to therapy at field strengths of 3T and above. Magnetization transfer (MT) is based on indirectly imaging semi-solid bound macromolecules (e.g., lipids of myelinated neurons). Chemical exchange saturation transfer (CEST) provides novel image contrast in MRI [7, 8] from exchangeable protons including those of mobile proteins. Specifically, amide proton transfer (APT) CEST [9], which relies on the saturation of the amide protons including those within peptide bonds, shows signals in brain tumors [10] related to increased levels of proteins and peptides [9, 11–13]. The APT CEST signal can differentiate pseudoprogression from true progression [14], separate radiation necrosis from tumor progression [15] and correlate with tumor grade and markers of cell proliferation [16, 17]. Specific to glioma, CEST studies at both 3T and 7T have suggested the potential to predict response to therapy [15, 18–20] and offer unique signal characteristics [21–23] and sensitivity to pH [24].

Prior to this study, CEST in brain tumors has not been performed below 3T. However, CEST at 1.5T would enable broader use in MR-guided radiotherapy systems [25, 26], including those with an integrated linear accelerator (LINAC) and on-board split bore MRI at 1.5T or lower field strengths [27]. Our previous work [28] extended in vivo CEST imaging to field strengths below 3T using a pulsed saturation method, but the study was limited to validation in the healthy brain and had not been performed in brain tumors. The aim of the present study was twofold: (i) to demonstrate that CEST can be performed in GBM at 1.5T and gives a reliable signal in tumors and (ii) to assess any differences between early and late progression cohorts, using CEST, qMT and other qMRI metrics in patients undergoing CRT, for determining the potential for response monitoring at 1.5T. Patients were imaged with CEST, MT, quantitative T_1-mapping and T_2-mapping MRI sequences at baseline (for treatment planning), after receiving the 10th and 20th fractions during the 6 weeks of CRT and lastly at 1 month post-CRT.

Methods

Study design

This prospective imaging study was approved by the Institutional Research Ethics Board. Patients were treated with standard of care radiation therapy consisting of 54–60 Gy over 30 fractions using intensity modulated radiotherapy (IMRT) concurrent with temozolomide. Radiation treatment was given once daily over 6 weeks excluding weekends and statutory holidays. The MRI sequences were determined a priori (Supplementary Table S1) at four time points—before radiation treatment ("Fx0") for treatment planning, at fraction 10 ("Fx10") and 20 ("Fx20") during CRT and at the 1 month timepoint following the final treatment fraction ("P1M") using a 1.5T Philips diagnostic MRI scanner. 51 consecutive patients were included in the analysis and the inclusion criteria are summarized in Supplementary Fig. S1.

Early or late progression

For each patient, tumor response was assessed and the time to progression, in number of days, from the Fx0 scan was recorded. Patients with tumors that progressed before or after 6.9 months (= 209 days) [3] were assigned to early and late progression categories, respectively. This time point was chosen based on the median PFS observed in patients treated with CRT on the Stupp trial [3]. Progression was defined based on the BRAIN-RANO response criteria for high-grade gliomas [29]. Late progression included patients who had stable imaging and clinical status at 6.9 months but who eventually relapsed.

MR imaging

MR imaging was conducted at 1.5T using an Ingenia diagnostic MRI (Philips Medical Systems, Best, Netherlands) with a 16-channel head coil. Standard clinical sequences included: pre-contrast T_1-weighted ("T_1w"), post-contrast T_1w ("T_1w + C"), FLAIR and DWI scans. A pulsed saturation sequence [28] was used for CEST/MT saturation to overcome the RF amplifier limitations. For CEST and MT, placement of the axial slice was based on identifying the largest extent of the tumor referenced on the first MRI time point. The WAter Shift And B1 (WASABI) sequence [30] was used for simultaneous pixelwise estimation of the B_1 scaling and B_0 frequency shift. T_1 mapping was performed

with a spoiled gradient echo sequence and T_2 mapping was performed with a T_2-weighted multi-echo sequence to obtain an observed T_2. The MR parameters are shown in Supplementary Table S1.

MT and CEST parameter fitting

Pulsed saturation data were fitted using the Bloch-McConnell equations with exact RF amplitudes and precise scan timings [31], with gradient spoiling accounted for using the EPG method as in previous work [28]. MT parameters included the semi-solid pool fraction (M_0^B) relative to water, the T_2 relaxation time of the semi-solid pool (T_2^B), the T_2 relaxation time of the water pool (T_2^A) and the exchange rate (R). CEST parameters included the CEST asymmetry, the magnetization transfer ratios MTR_{Amide} and MTR_{NOE} [18] and, after removing the MT contributions using previous extrapolation methods [28, 32, 33], the amide and nuclear Overhauser effects (NOE) areas. The CEST signal was averaged between 2 and 4 ppm, and the Z-spectra from the two nominal RF amplitudes (acquired at 1.5 and 3 μT) were interpolated to 2.5 μT. To generate the asymmetry maps, the z-spectra were centered (voxelwise) using the estimated B_0 before quantification between 2 and 4 ppm. This large frequency offset range was used to increase SNR. Detailed methods and the processing pipeline to derive each parameter are described in a previous study that included CEST scans at 1.5T in a healthy subject [28]. CEST z-spectra are provided, where differences between the positive and negative side of the z-spectra were plotted to display the asymmetry. Numerical simulations were processed using MATLAB v2016b (The MathWorks, Natick, MA).

Image registration

The post-contrast T_1-weighted and FLAIR volumes were rigidly co-registered to the first pre-contrast T_1 volume (at Fx0) for each subsequent time point (i.e., Fx10, Fx20 and P1M) using FSL (FMRIB, Oxford, UK; http://www.fmrib.ox.ac.uk/fsl) [34]. For the CEST scans, rigid 2D motion correction was performed using FSL prior to parameter estimation. Slices that corresponded to the scanned CEST/MT slices were extracted from the T_1-weighted and FLAIR volumes.

Regions of interest (ROIs)

Radiotherapy ROIs included the gross tumor volume (GTV) and clinical target volume (CTV), which were drawn separately at each imaging time point (Fx0/Fx10/Fx20/P1M) on the post-contrast T_1-weighted volumes for each patient. The GTV included the residual gross tumor and surgical cavity. The CTV was delineated by applying a 1.5 cm volumetric expansion beyond the GTV while respecting normal anatomic boundaries to tumor routes of spread. The GTV and CTV contours from each time point were registered to those of the Fx0 imaging volumes by applying the identical transformation that resulted from the registration of each Fx10/Fx20/P1M set of images to the Fx0 scan. These contours were then modified by excluding voxels outside of the brain and ventricles to remove confounding contributions from cerebrospinal fluid. Future instances of "GTV" and "CTV" will refer to these modified contours.

Volumetric contours representing the T_1C-enhancing (T_1C_{ENH}) region and the FLAIR-hyperintense ($FLAIR_{HYP}$) regions were contoured based on the 3D T_1w+C and 3D FLAIR images, by manual segmentation assisted by automatic thresholding using AMIRA Software (v2019.2, Thermo Fisher Scientific), excluding necrotic areas and hemorrhagic tissue within the surgical cavity. Areas of intrinsic T_1 hyperintensity, representative of hemorrhagic material, was excluded for T_1C_{ENH} contours by slice-by-slice comparison with pre-contrast images during contouring, and verified by a neuroradiologist with 9 years of experience. The T_1C_{ENH} regions were excluded from the $FLAIR_{HYP}$ contours so that the regions do not overlap. The resection cavities within the enhancing rim were included in the CTV and GTV regions, but were manually excluded from the T_1C_{ENH} and $FLAIR_{HYP}$ regions. The contours at the CEST/MT slice were extracted for analysis. Contours without enhancement, or those that did not overlap with the CEST/MT slices, were excluded from analysis (see Supplementary Fig. S2). In addition, regions in the contralateral normal appearing white matter (cNAWM) were drawn for the slice of interest, ensuring no overlap with the tumor.

Statistical analysis

Parameter value differences

Comparisons were performed between (i) GTV and cNAWM, and (ii) early and late progression cohorts. Differences in parameter values between the GTV and cNAWM were compared with Wilcoxon signed-rank tests and corrected for multiple testing with the Hommel method [35]. Differences in parameter values between early and late progression were individually assessed for each parameter and ROI combination with linear mixed effect models. Mean parameter value differences between early and late progression were modelled as a fixed effect. Changes in mean value differences at different time points were also modelled as a fixed effect using an interaction term with time as a categorical variable. Individual subjects were modelled as a random effect on the intercept representing the parameter value at Fx0. Between early and late cohorts, multiple testing adjustment was not performed due to the hypothesis-generating

nature of this study [36]. An alpha threshold of 0.05 was used for statistical significance.

Exploratory predictive modelling

Each unique parameter, ROI and timepoint combination was considered to be a potential predictor of early vs. late progression status. An initial univariate selection of potential predictors was done using a *p* value threshold of 0.05 for entry into the multivariable predictive model. Missing values for significant predictors were imputed using multivariable imputation by chained equations [37] (package "mice" v3.9.0) before multivariable modelling. We used the model selection and averaging techniques published by Schomaker and Heumann [38] (package "MAMI" 0.9.13) to obtain the exploratory predictive model, accounting for multiple imputation. The following parameters were used for the model selection algorithm: model = "binomial", method = "LASSO", kfold (k-fold cross validation to tune the Lambda hyperparameter in the "glmnet" package [version 4.0-2]) = 10, cvr = FALSE (no shuffling of validation sets for reproducibility), CI 0.95 (95% confidence interval) and inference = "+boot" (bootstrap confidence interval construction), with B = 100 (number of bootstrap replications). Default values were accepted for other parameters. Exploratory multivariable predictive models were evaluated using the Hosmer–Lemeshow test, its concordance (C)-statistic and accuracy to demonstrate feasibility. After the model based on qMRI predictors with the best performance was generated, five additional clinical characteristics including age, sex, extent of resection, O^6-methylguanine-DNA-methyltransferase (MGMT) methylation status and isocitrate dehydrogenase (IDH) mutation status, specifically the IDH1-R132H status, were added to qMRI-based model one by one. Any clinical characteristic that significantly contributed to the model was retained. All statistical analysis was carried out in R (v3.6.2 x64: R Core Team (2019), Vienna, Austria).

Results

In this prospective study, 15/51 (29.4%) had a gross total resection (GTR) with the remaining having had a subtotal resection (STR) (28/51 = 54.9%) or stereotactic biopsy only (8/51 = 15.7%). One patient was treated on the basis of radiographic features consistent with a high-grade glioma. 48/51 (94.1%) did not have the IDH1-R132H mutation (wild type) and 21/51 (41.2%) were O^6-methylguanine-DNA-methyltransferase (MGMT) promoter unmethylated. At baseline, 23 patients progressed within 6.9 months (i.e., early progression) and 28 represented the late progression cohort. One patient (with unknown MGMT status, who was imaged only at baseline) developed rapid clinical decline and received 10 fractions. Table 1 summarizes the patient and tumor characteristics.

In Fig. 1a, example maps of the T_1, T_2, MT semi-solid fraction (M_0^B), CEST asymmetry and the CEST amide magnetization transfer ratio (MTR_{Amide}) are shown. Compared to surrounding brain regions, the tumor exhibited greater T_1, T_2 and CEST asymmetry, and lower MT semi-solid fraction and MTR_{Amide}. On the post-contrast T_1-weighted images, the residual enhancing surgical bed evolved with greater peripheral enhancement surrounding an area of central necroses at the last two time points (Fx20 and P1M). The extent of peritumoral edema visualized on the FLAIR images also

Table 1 Patient characteristics: clinical details of patients included in the analysis are shown, including age, sex, tumor location, gross tumor volume, resection status, isocitrate dehydrogenase (IDH) mutation and O^6-methylguanine-DNA-methyltransferase (MGMT) promoter methylation status

Variable	Data
Number of patients	51
Age (years)	
Median	56
Range	19–68
Sex	
Male	29
Female	22
Tumor location by lobe	
Parietal	10
Frontal	14
Temporal	17
Occipital	2
Other	8
Tumor location by hemisphere	
Left	27
Right	18
Bilateral or central	6
Gross tumor volume at baseline (cc)	
Median	19.8
Range	1.1 – 141.2
Resection status	
Subtotal resection (STR)	28
Gross total resection (GTR)	15
Not resected or Biopsied	8
IDH mutation status	
Wild type	48
Mutant	2
Unknown	1
MGMT methylation status	
Methylated	24
Unmethylated	21
Unknown	6

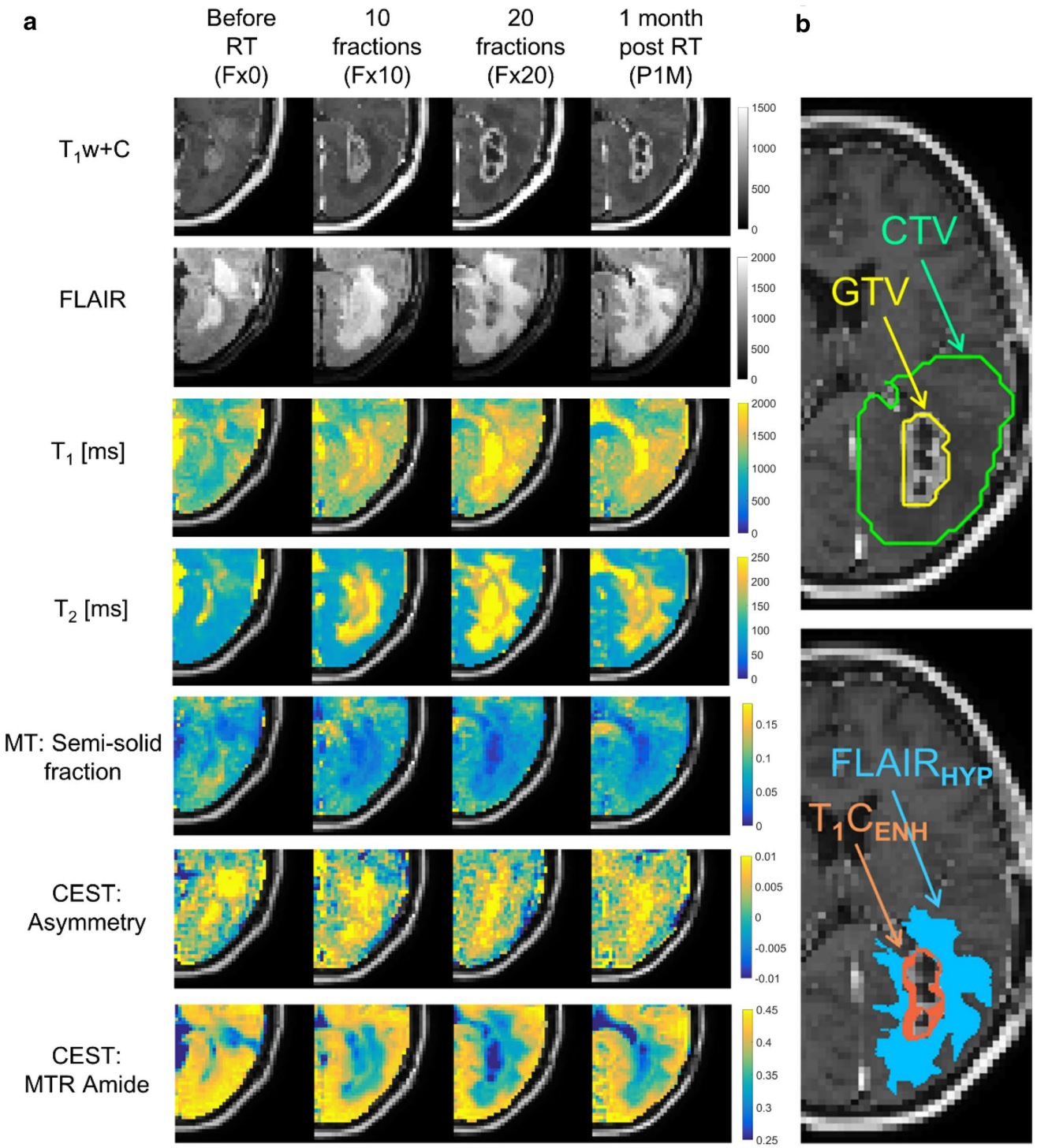

Fig. 1 Example quantitative parameter maps and regions of interest: **a** Standard clinical images are shown including the post-contrast T_1-weighted (T_1w+C) and FLAIR images. Quantitative maps are shown for the T_1 relaxation time, T_2 relaxation time, MT semi-solid fraction (M_0^B), CEST asymmetry and the CEST amide magnetization transfer ratio. Images are shown for all four imaging time points (before radiation therapy, at 10 fractions, at 20 fractions and 1 month after the last treatment fraction) of a patient who had late progression (i.e., after 6.9 months). **b** Radiotherapy contours for the gross tumor volume (GTV) and clinical target volume (CTV) are shown at 1 month after the end of radiation therapy for the same example case (outlined in yellow and green, respectively). The contours shown have been modified compared to the original GTV and CTV by excluding the ventricle and skull regions. T_1C-enhancing (T_1C_{ENH}) and FLAIR-hyperintense ($FLAIR_{HYP}$) regions are represented by the shaded areas (in orange and blue, respectively)

changed; in particular, from the baseline to Fx10. Figure 1b illustrates the standard GTV and CTV contours, and the T_1C_{ENH} and $FLAIR_{HYP}$ (which excluded necrotic tumor regions and the surgical cavity).

Compared to cNAWM, tumors had significantly higher median T_1 and T_2, lower MT semi-solid fractions, and higher CEST asymmetry at all time points, as shown in Fig. 2. Except for T_2^B, exchange rate (R), the CEST NOE area (for all time points) and the amide area (for the Fx20 and P1M), all qMRI values were significantly different between the GTV and cNAWM regions for all time points ($p < 0.001$ after Hommel correction for multiple testing).

Comparisons of the qMRI values between early and late progression cohorts are provided in Fig. 3. The baseline CEST asymmetry in the CTV was significantly higher in early progression compared to late progression (unadjusted $p = 0.003$). Other significantly different parameters included the T_1 relaxation time (at Fx0), semi-solid T_2^B (at Fx20), water pool T_2^A (at P1M) and the exchange rate (at Fx20). Baseline maps of representative subjects are provided in Supplementary Figure S3 for the MT semi-solid fraction, CEST asymmetry and amide area. To illustrate the reliability of detecting a CEST signal at 1.5T in GBM tumors, zoomed-in CEST asymmetry maps for the first 10 patients are provided in Supplementary Fig. S4. As shown, the CEST asymmetry maps at 1.5T are visually distinct between patients, with consistent spatial signatures across the time points and with some signal changes seen over the course of therapy. In Supplementary Fig. S5, it can be seen that the CEST asymmetry, although small (relative to higher field strengths or when continuous RF saturation can be used), is detectable and is visible on the CEST z-spectra. Spatial variations of the signal were observed; an example is shown of a tumor that had two regions with differing intensities on the CEST asymmetry map. The z-spectra are shown separately for these tumor regions and for cNAWM, which exhibited lower asymmetry.

A summary of the parameter differences across all qMRI metrics is provided in Fig. 4a. ROC curves from the exploratory predictive modelling are shown in Fig. 4b (computed with qMRI parameters only) and Fig. 4c (with added clinical factors). With qMRI parameters only, three potential predictors that may indicate early tumor progression were found (CEST asymmetry, the semi-solid T_2^B and the exchange rate at the ROIs and time points listed in Fig. 4b), resulting in a maximum predictive accuracy of 0.79 for early progression status (95% confidence interval: 0.78–0.79), with a C-statistic of 0.84 (95% CI 0.84–0.85). When MGMT methylation status was added, the predictive accuracy improved to 0.87 (95% CI 0.86–0.87) with a C-statistic of 0.87 (95% CI 0.87–0.88). Unmethylated MGMT significantly increased the odds of early progression, with an odds ratio of 3.93 (95% CI 1.00–30.9). Conversely, MGMT status alone was a poor predictor of early progression status without qMRI predictors (Fig. 4c). In this cohort, age, sex, extent of resection and IDH mutation status did not augment the model.

Discussion

This study investigated CEST/MT as part of a 1.5T qMRI protocol in 51 patients with GBM undergoing CRT. Our study builds upon previous studies at 3T [18, 39], and furthers it to qMRI metrics including CEST at 1.5T for which the GBM tumor signal had not previously been quantified. Differences between early and late progressors show promise for these qMRI metrics to be used as non-invasive imaging biomarkers of biologic response. The differences were found to vary across the regions, likely owing to the spatial heterogeneity within GBM tumors. Differences between the T_1C_{ENH} contour and the GTV were most likely driven by the necrotic regions and also, for resected tumors, the surgical cavities, that were part of the GTV (and CTV) but which were excluded from the T_1C_{ENH} (and $FLAIR_{HYP}$) regions.

Significant differences between the GTV and cNAWM signals included the CEST asymmetry and amide area (for Fx0 and Fx10), confirming the detectability of CEST signal changes in GBM even at 1.5T. As reported [18], the CEST signal patterns differed from other maps, suggesting that CEST may be providing additional metabolic information. The lack of significant differences in the amide area at Fx20 and P1M could be related to previous findings [40] of altered signals in the cNAWM in GBM patients compared to healthy brain tissue. For MT, lower semi-solid fractions in tumors are likely related to the loss of white matter resulting in a different macromolecular composition compared to the normal brain [41, 42].

The baseline CEST asymmetry (in CTV) differentiated between early and late progression. This is in accordance with pre-treatment measurements from previous studies (one performed at 3T [18] and two performed at 7T [19, 20]), which showed significantly higher APT in patients with early progression. Similar to mixed modelling results, exploratory predictive modelling also identified CEST asymmetry as a predictor at baseline (Fx0) in the CTV. Signal changes after the start of CRT did not reveal any CEST metrics to be different between early and late progression cohorts, similarly observed in a previous study [18]. No significant differences were seen in the NOE parameters between early and late progression cohorts. Previous experiments performed in the healthy brain demonstrated that the relayed NOE was decreased at 1.5T compared to 3T [28]. High APT signals are speculated to be related to an increased proportion of small protein fragments and peptides [11, 19], with pH suggested to

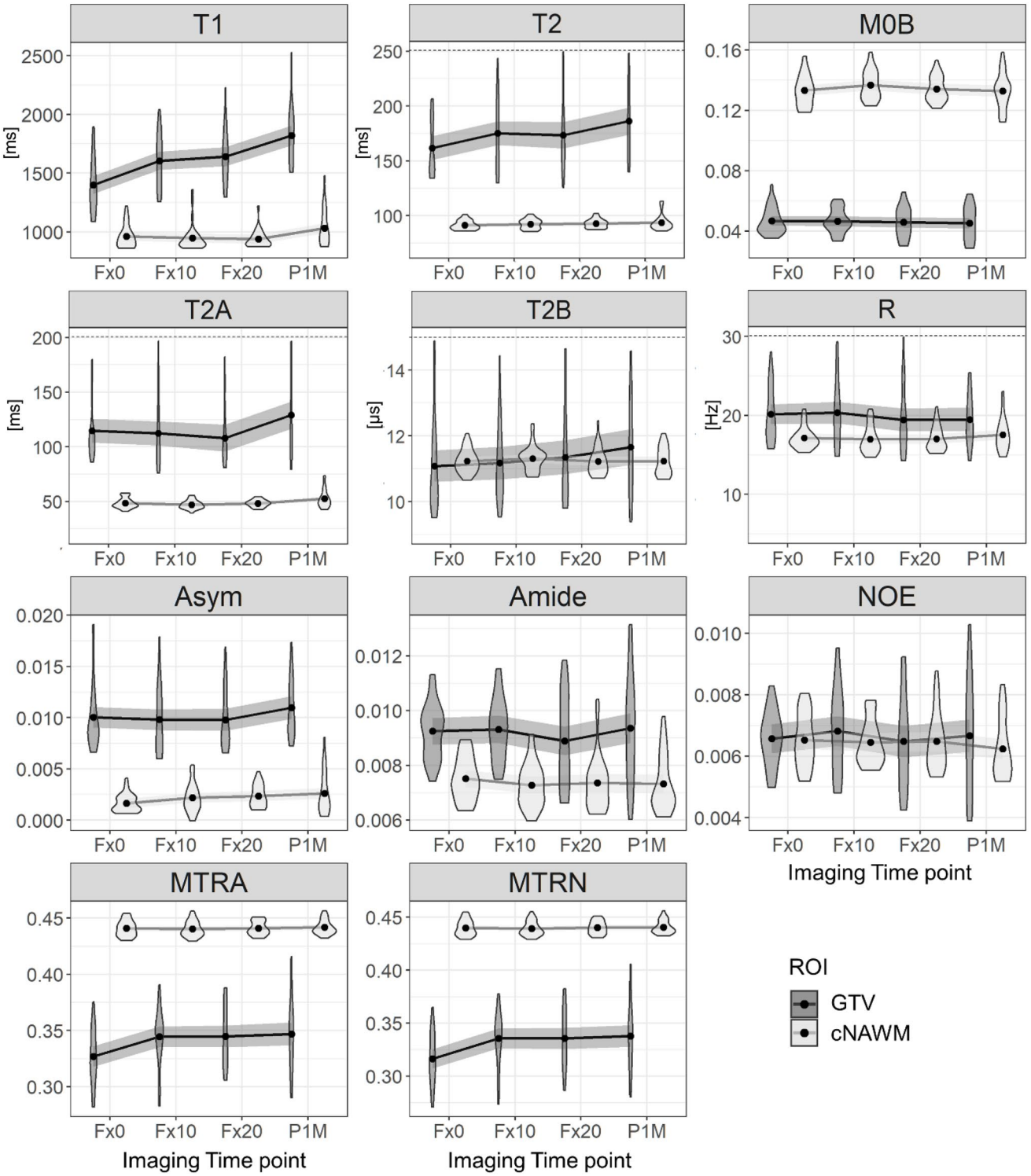

Fig. 2 Comparison between GTV tumor and cNAWM regions: Mean values (represented by black dots) over the entire patient cohort in the gross tumor volume (GTV) and contralateral normal appearing white matter (cNAWM) regions are shown for 11 parameter maps: T_1, T_2, the MT parameters (semi-solid fraction "M0B", T_2 relaxation of the water pool "T2A", T_2 relaxation of the semi-solid pool "T2B" and exchange rate "R") and the CEST parameters (asymmetry "Asym", amide area "Amide", NOE area "NOE", magnetization transfer ratio for amide "MTRA" and for NOE "MTRN") across the four imaging time points (Fx0, Fx10, Fx20 and P1M). The lines show the smoothed means with 95% confidence interval. Top and bottom 2.5th percentiles of the violin plots are trimmed

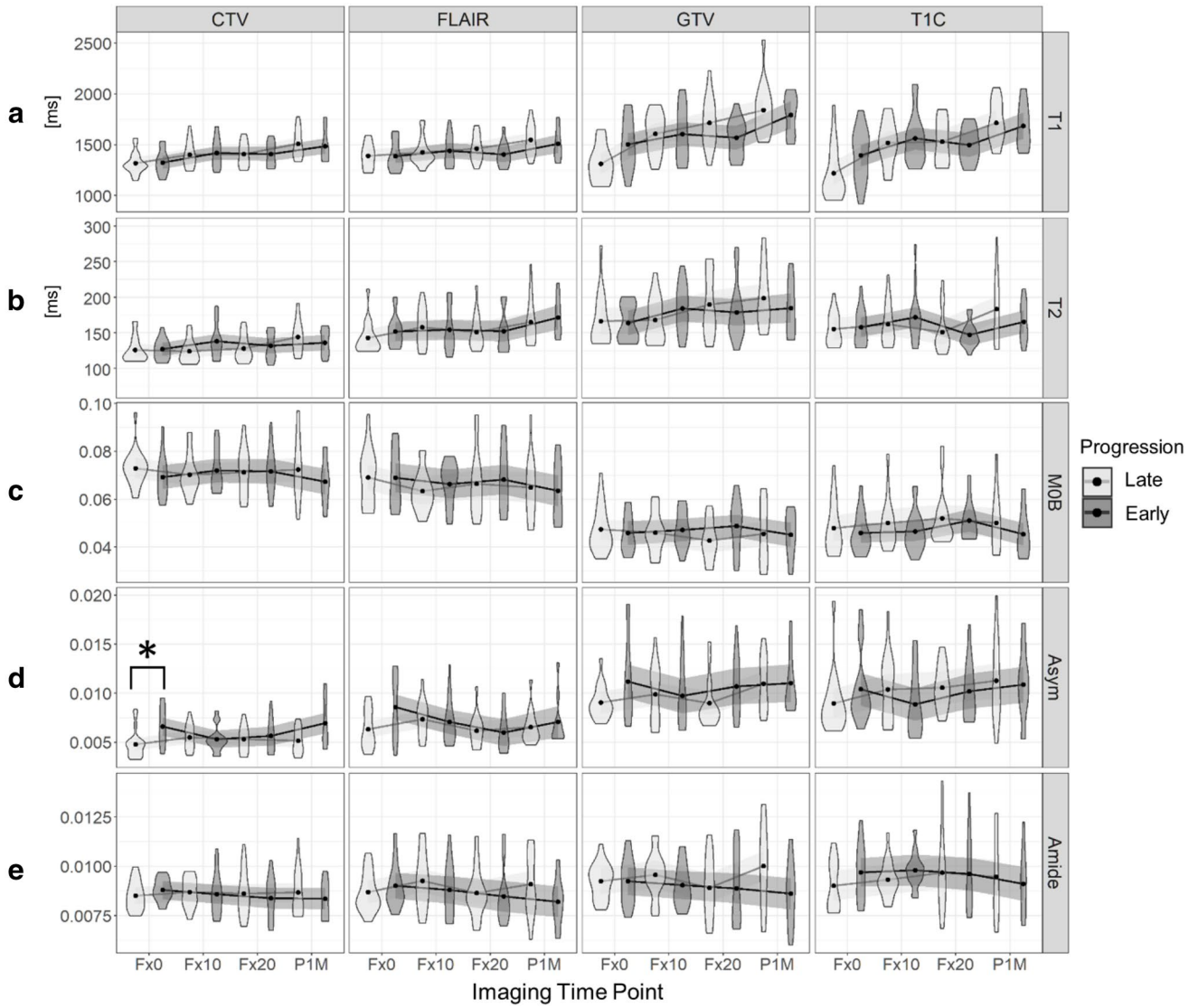

Fig. 3 Early and Late tumor progression: The mean values with violin plots for the early (dark grey) and late (light grey) progression cohorts are shown for a subset of the parameters **a** T_1, **b** T_2, **c** MT semi-solid fraction "M_0^B", **d** CEST asymmetry "Asym" and **e** amide area "Amide", for each ROI (CTV, $FLAIR_{HYP}$, GTV, T_1C_{ENH}) over the four time points (Fx0, Fx10, Fx20 and P1M). The lines show smoothed means with 95% confidence interval. Top and bottom 2.5th percentiles of the violin plots are trimmed

have less contribution [19, 43, 44]. The underlying causes of CEST signal changes due to therapy remains an active area of research.

For MT, previous work [39] at 3T reported higher baseline fractions with minimal subsequent change after treatment in patients with early progression, compared to larger increases in late progression after treatment. In our study, several MT parameters differentiated between early and late progression, with exploratory predictive modelling identifying T_2^B and the exchange rate as predictors. Interestingly, the semi-solid fraction was not identified as a significant predictor, which could be related to correlations between the MT parameters.

Increasing T_1 and T_2 relaxation times in tumor GTV values during treatment were consistent with a previous report [45]. The baseline pre-contrast T_1 relaxation time in the T_1C_{ENH} region differentiated between early and late progression. Studies comparing the pre- and post-gadolinium T_1 maps found that an early volume decrease in the "cloudy-enhancing" tumor compartment predicted longer PFS [46], which warrants further investigation of T_1 mapping for treatment monitoring.

Exploratory predictive modelling showed that both qMRI and clinical factors were required to achieve maximum predictive accuracy for early progression. CEST asymmetry, MT metrics (i.e., T_2^B, R) and MGMT status were significant

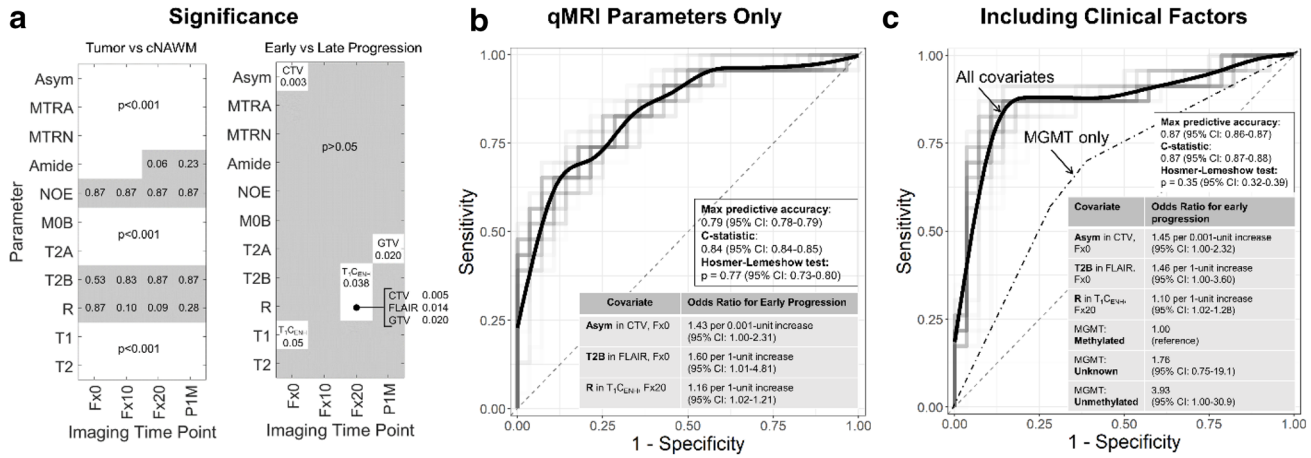

Fig. 4 Parameter differences and exploratory predictive modelling: **a** Significant differences between tumor (GTV) and cNAWM are shown on the left. White boxes indicate significant parameters and the p values are shown after Hommel correction for multiple testing. Parameter differences between early and late progression are shown on the right, with white boxes indicating significant parameters for specific ROIs with unadjusted p values. **b** The ROC curve representing the best-performing predictive model with qMRI parameters only, with overall model diagnostics (C-statistic, predictive accuracy) and the odds ratio estimates for each parameter are shown. **c** A similar ROC curve is shown, representing the best-performing predictive model with both qMRI parameters and the clinical parameter of MGMT methylation status. Grey: superimposition of individual ROC curves for each of the 100-fold imputed datasets. Black: a single smoothed curve summarizing the individual ROC curves. Dotted black line: for comparison, the ROC curve is shown where only one of the clinical factors, the MGMT methylation status, was used as a predictor for early progression (a max predictive accuracy of 64.7%, C-statistic: 0.663, and Hosmer–Lemeshow test: $p < 0.001$ for MGMT only)

predictors, with time points of significance at baseline and at Fx20. The implications of early identification of progression could be to abandon treatment in cases of clinical deterioration, to switch therapy, dose escalate the radiotherapy regimen, and inform the participation in clinical trials or reoperation. This study suggests potential for qMRI to better inform patient care such that eventually clinical practice becomes personalized to an individual's tumor [25].

This study has a number of limitations. First, a single slice was used for the saturation sequences, which may introduce errors in slice positioning. More accurate positioning is achievable on the MR Linac Elekta Unity (Elekta AB, Stockholm, Sweden) where the patient is immobilized and indexed to the radiation unit [27], and with the implementation of 3D techniques. It remains challenging to extract only the APT signal and there could have been residual influences from non-CEST parameters. There also could have been contributions from overlapping metabolites [47], especially with reduced spectral separation at 1.5T compared to at 3T, as well as the wider frequency offset range of 2–4 ppm used in the quantification to increase SNR. In the GTV and CTV contours, hemorrhagic regions within the surgical cavity, possibly unrelated to radiation treatment, could have influenced the signal. Hemorrhagic changes are known to cause changes in the T_1 and T_2 [48], and indirectly, this could have affected the MT and CEST signals. The CEST signal between early and late progression cohorts were seen to have substantial overlap at the individual subject level. Compared to a 3T GBM study comparing progressors and non-progressors [18], there was greater overlap at 1.5T. More investigation will be needed to determine whether CEST, although reliable for detecting a tumor signal at 1.5T, could be used to distinguish between these cohorts on an individual patient level. Contributors of this overlap may include differing tumor location, resection status and genetic subtype. The ability of CEST alone, without other qMRI variables, for distinguishing early and late progression remains to be confirmed in larger studies. However, good differentiation between tumor and cNAWM tissue demonstrates that a reliable tumor signal can be obtained using CEST at 1.5T.

Since the resection cavity was excluded from the T_1C_{ENH} and $FLAIR_{HYP}$ contours, subjects with GTR compared to STR would likely have fewer voxels remaining in the T_1C_{ENH} and $FLAIR_{HYP}$ regions for analysis, and may cause the median values to be less representative. For the GTV and CTV regions (which had included resection cavities), the size and contents of the cavity (including hemorrhagic tissue) would influence the signal for all qMRI parameters. Although the qMT semi-solid fractions are relatively low near or within the resection cavity, the CEST signal may be affected by protein and peptide levels, or pH changes within the cavity.

Although this study comprised the largest sample size of its kind to date, external validation in larger cohorts such as a multi-institutional consortium [49] are critical to improve the reliability of future models. The end points of this study

were assessed according to the RANO criteria [29]; pseudoprogression was taken into account when determining the time point of early or late progression. However, we note the limitations of the RANO criteria; improvements have been suggested [50] including the use of volumetric response assessment, which can be considered in future studies. Survival analysis was not performed as it would require larger sample sizes given the number of covariates used in this study to achieve meaningful results. Our current findings, which are focused on response prediction, support the need to continue this prospective imaging study where the prognostic value would be analyzed in larger sample sizes with sufficient statistical power. A certain level of bias was accepted, given the exploratory nature of our study and the need for further validation. Our approach using multiple imputation with a LASSO-based logistic regression with L1 regularization penalty, was chosen to reduce bias compared to conventional and more prevalent logistic regression approaches. The predictive power of these biomarkers should be interpreted with caution due to the limited sample size for the number of predictors used. We emphasize the exploratory nature of this early-phase study where the goal was to demonstrate the ability of a 1.5T MRI in producing images of sufficient quality for future biomarker analysis when we have a larger sample size.

Future directions will involve applying a radiomics framework and incorporating next generation sequencing information. It would be beneficial to include other clinical data such as surrogate markers of the extent of residual disease at the time of surgery or the tumor cell concentration. In addition, consensus radiotherapy contours could be used for quantification [51]. The optimal imaging time point to reflect tumor response remains an area of investigation, and greater insights could be gained by multiparametric qMRI on the MR-Linac.

Conclusions

Multiparametric qMRI including CEST and MT acquired at 1.5T was shown to be a potential biomarker for tracking the functional and metabolic changes in GBM during CRT. This study demonstrated for the first time that CEST signals in GBM tumors are detectable at 1.5T, and together with qMRI parameters, was associated with tumor progression.

Acknowledgements We gratefully acknowledge the following sources of funding: Natural Sciences and Engineering Research Council (NSERC); the Terry Fox Research Institute; Canadian Institutes of Health Research; the Canadian Cancer Society Research Institute. We thank Mikki Campbell for coordinating the study and we thank the MR radiation therapists who were involved in scanning: Helen Su, Ling Ho, Katie Wong, Monica Foster, Danny Yu, Lin Lu, Amy Pham-Chau and Khang Vo. We also thank Guillaume Gilbert for helpful advice related to Philips pulse programming.

Author contributions Conceptualization: RWC, SM, GJS, GJC, AS, AZL; Data curation: RWC, SM, JS, PJM, AKMC, S.Daghighi, MR, AZL; Formal analysis: RWC, HC, EGA, AZL; Funding acquistion: GJS, GJC, AS, AZL; Investigation: RWC, HC, SM, EGA, AZL; Methodology: RWC, HC, EGA, GJS, AZL; Project administration: RWC, AS, AZL; Resources: GJS, GJC, S.Das, AS, AZL; Software: RWC, HC, JS, PJM, AKMC, S.Daghighi, AZL; Supervision: GJS, GJC, AS, AZL; Validation: RWC, HC, EGA, GJS, AZL; Visualization: RWC, HC, AZL; Writing—original draft: RWC, HC, AZL; Writing—review and editing: RWC, HC, SM, EGA, GJS, JS, PJM, AKMC, S.Daghighi, MR, S.Das, JP, GJC, AS, AZL.

Funding This research received support from Natural Sciences and Engineering Research Council (NSERC) (RGPIN-2017-06596, CRD 507521-16); the Terry Fox Research Institute (TFRI Project 1034), Terry Fox (New Frontiers Program Project Grant); Canadian Institutes of Health Research (CIHR 156252, 148660); the Canadian Cancer Society Research Institute (CCSRI 701640, CCSRI 705083).

Code availability Will be available upon request.

Compliance with ethical standards

Conflicts of interest Dr. Arjun Sahgal has been an advisor/consultant with Abbvie, Merck, Roche, Varian (Medical Advisory Group), Elekta (Gamma Knife Icon), BrainLAB, and VieCure (Medical Advisory Board); received honorarium for past educational seminars with Elekta AB, Accuray Inc., Varian (CNS Teaching Faculty), BrainLAB and Medtronic Kyphon; research grant with Elekta AB; received travel accommodations/expenses by Elekta, Varian and BrainLAB. Dr. Sten Myrehaug has received research support from Novartis AG, honoraria from Novartis AG and Ipsen and travel support from Elekta; No conflicts of interest related to this work. Dr. Mark Ruschin is a co-inventor of and owns associated intellectual property specific to the image-guidance system on the Gamma Knife Icon. No conflicts of interest related to this work. Dr. Sunit Das has received grant support from Alkermes plc and honoraria for advisory board activities from Subcortical Surgery Group. The rest of the authors have no conflicts of interest to declare that are relevant to the content of this article.

Consent to participate and for publication No informed consent was required as the data was anonymized and the submission does not include images that may identify the subjects.

Ethics approval This study was approved by the Institutional Research Ethics Board at Sunnybrook Health Sciences Centre.

References

1. Darefsky AS, King JT, Dubrow R (2012) Adult glioblastoma multiforme survival in the temozolomide era: a population-based analysis of Surveillance, Epidemiology, and End Results registries. Cancer 118:2163–2172. https://doi.org/10.1002/cncr.26494
2. Koshy M, Villano JL, Dolecek TA et al (2012) Improved survival time trends for glioblastoma using the SEER 17

population-based registries. J Neurooncol. https://doi.org/10.1007/s11060-011-0738-7
3. Stupp R, Mason WP, Van Den Bent MJ et al (2005) Radiotherapy plus concomitant and adjuvant temozolomide for glioblastoma. N Engl J Med 352:987–996. https://doi.org/10.1056/NEJMoa043330
4. Wolff SD, Balaban RS (1989) Magnetization transfer contrast (MTC) and tissue water proton relaxation in vivo. Magn Reson Med 10:135–144. https://doi.org/10.1002/mrm.1910100113
5. Henkelman RM, Huang X, Xiang Q-S et al (1993) Quantitative interpretation of magnetization transfer. Magn Reson Med 29:759–766. https://doi.org/10.1002/mrm.1910290607
6. Wolff SD, Balaban RS (1990) NMR imaging of labile proton exchange. J Magn Reson 86:164–169. https://doi.org/10.1016/0022-2364(90)90220-4
7. Ward KM, Aletras AH, Balaban RS (2000) A new class of contrast agents for MRI based on proton chemical exchange dependent saturation transfer (CEST). J Magn Reson 143:79–87. https://doi.org/10.1006/jmre.1999.1956
8. van Zijl PCM, Lam WW, Xu J et al (2018) Magnetization transfer contrast and chemical exchange saturation transfer MRI. Features and analysis of the field-dependent saturation spectrum. Neuroimage 168:222–241. https://doi.org/10.1016/j.neuroimage.2017.04.045
9. Zhou J, Lal B, Wilson DA et al (2003) Amide proton transfer (APT) contrast for imaging of brain tumors. Magn Reson Med 50:1120–1126. https://doi.org/10.1002/mrm.10651
10. Jones CK, Schlosser MJ, Van Zijl PCM et al (2006) Amide proton transfer imaging of human brain tumors at 3T. Magn Reson Med 56:585–592. https://doi.org/10.1002/mrm.20989
11. Hobbs SK, Shi G, Homer R et al (2003) Magnetic resonance image-guided proteomics of human glioblastoma multiforme. J Magn Reson Imaging 18:530–536. https://doi.org/10.1002/jmri.10395
12. Howe FA, Barton SJ, Cudlip SA et al (2003) Metabolic profiles of human brain tumors using quantitative in vivo 1H magnetic resonance spectroscopy. Magn Reson Med 49:223–232. https://doi.org/10.1002/mrm.10367
13. Zhou J (2010) Amide proton transfer imaging of the human brain. Methods Mol Biol. https://doi.org/10.1007/978-1-61737-992-5_10
14. Ma B, Blakeley JO, Hong X et al (2016) Applying amide proton transfer-weighted MRI to distinguish pseudoprogression from true progression in malignant gliomas. J Magn Reson Imaging. https://doi.org/10.1002/jmri.25159
15. Mehrabian H, Desmond KL, Soliman H et al (2017) Differentiation between radiation necrosis and tumor progression using chemical exchange saturation transfer. Clin Cancer Res 23:3667–3675. https://doi.org/10.1158/1078-0432.CCR-16-2265
16. Togao O, Yoshiura T, Keupp J et al (2014) Amide proton transfer imaging of adult diffuse gliomas: correlation with histopathological grades. Neuro Oncology 16:441–448. https://doi.org/10.1093/neuonc/not158
17. Park JE, Kim HS, Park KJ et al (2016) Pre-and posttreatment glioma: comparison of amide proton transfer imaging with MR spectroscopy for biomarkers of tumor proliferation. Radiology 278:514–523. https://doi.org/10.1148/radiol.2015142979
18. Mehrabian H, Myrehaug S, Soliman H et al (2018) Evaluation of glioblastoma response to therapy with chemical exchange saturation transfer. Int J Radiat Oncol Biol Phys 101:713–723. https://doi.org/10.1016/j.ijrobp.2018.03.057
19. Regnery S, Adeberg S, Dreher C et al (2018) Chemical exchange saturation transfer MRI serves as predictor of early progression in glioblastoma patients. Oncotarget 9:28772–28783. https://doi.org/10.18632/oncotarget.25594
20. Meissner JE, Korzowski A, Regnery S et al (2019) Early response assessment of glioma patients to definitive chemoradiotherapy using chemical exchange saturation transfer imaging at 7 T. J Magn Reson Imaging 50:1268–1277. https://doi.org/10.1002/jmri.26702
21. Zaiss M, Windschuh J, Paech D et al (2015) Relaxation-compensated CEST-MRI of the human brain at 7T: unbiased insight into NOE and amide signal changes in human glioblastoma. Neuroimage 112:180–188. https://doi.org/10.1016/j.neuroimage.2015.02.040
22. Zaiss M, Windschuh J, Goerke S et al (2017) Downfield-NOE-suppressed amide-CEST-MRI at 7 Tesla provides a unique contrast in human glioblastoma. Magn Reson Med 77:196–208. https://doi.org/10.1002/mrm.26100
23. Paech D, Zaiss M, Meissner JE et al (2014) Nuclear overhauser enhancement mediated chemical exchange saturation transfer imaging at 7 tesla in glioblastoma patients. PLoS ONE 9:3–9. https://doi.org/10.1371/journal.pone.0104181
24. Harris RJ, Yao J, Chakhoyan A et al (2018) Simultaneous pH-sensitive and oxygen-sensitive MRI of human gliomas at 3 T using multi-echo amine proton chemical exchange saturation transfer spin-and-gradient echo echo-planar imaging (CEST-SAGE-EPI). Magn Reson Med 80:1962–1978. https://doi.org/10.1002/mrm.27204
25. Cao Y, Tseng CL, Balter JM et al (2017) MR-guided radiation therapy: transformative technology and its role in the central nervous system. Neuro Oncology 19:ii16–ii29. https://doi.org/10.1093/neuonc/nox006
26. Raaymakers BW, Jürgenliemk-Schulz IM, Bol GH et al (2017) First patients treated with a 1.5 T MRI-Linac: clinical proof of concept of a high-precision, high-field MRI guided radiotherapy treatment. Phys Med Biol 62:L41–L50. https://doi.org/10.1088/1361-6560/aa9517
27. Hall WA, Paulson ES, van der Heide UA et al (2019) The transformation of radiation oncology using real-time magnetic resonance guidance: a review. Eur J Cancer 122:42–52. https://doi.org/10.1016/j.ejca.2019.07.021
28. Chan RW, Myrehaug S, Stanisz GJ et al (2019) Quantification of pulsed saturation transfer at 1.5T and 3T. Magn Reson Med 82:1684–1699. https://doi.org/10.1002/mrm.27856
29. Wen PY, Macdonald DR, Reardon DA et al (2010) Updated response assessment criteria for high-grade gliomas: response assessment in neuro-oncology working group. J Clin Oncol 28:1963–1972. https://doi.org/10.1200/JCO.2009.26.3541
30. Schuenke P, Windschuh J, Roeloffs V et al (2017) Simultaneous mapping of water shift and B 1 (WASABI)—application to field-Inhomogeneity correction of CEST MRI data. Magn Reson Med 77:571–580. https://doi.org/10.1002/mrm.26133
31. Graham SJ, Henkelman RM (1997) Understanding pulsed magnetization transfer. J Magn Reson Imaging. https://doi.org/10.1002/jmri.1880070520
32. Heo HY, Zhang Y, Lee DH et al (2016) Quantitative assessment of amide proton transfer (APT) and nuclear overhauser enhancement (NOE) imaging with extrapolated semi-solid magnetization transfer reference (EMR) signals: application to a rat glioma model at 4.7 tesla. Magn Reson Med 75:137–149. https://doi.org/10.1002/mrm.25581
33. Lam WW, Oakden W, Murray L et al (2018) Differentiation of normal and radioresistant prostate cancer xenografts using magnetization transfer-prepared MRI. Sci Rep 8:6–15. https://doi.org/10.1038/s41598-018-28731-0
34. Jenkinson M, Beckmann CF, Behrens TEJ et al (2012) FSL. Neuroimage 62:782–790. https://doi.org/10.1016/j.neuroimage.2011.09.015

35. Hommel G (1988) A stagewise rejective multiple test procedure based on a modified bonferroni test. Biometrika. https://doi.org/10.1093/biomet/75.2.383
36. Bender R, Lange S (2001) Adjusting for multiple testing—when and how? J Clin Epidemiol 54:343–349. https://doi.org/10.1016/S0895-4356(00)00314-0
37. van Buuren S, Groothuis-Oudshoorn K (2011) mice: multivariate imputation by chained equations in R. J Stat Softw. https://doi.org/10.18637/jss.v045.i03
38. Schomaker M, Heumann C (2014) Model selection and model averaging after multiple imputation. Comput Stat Data Anal. https://doi.org/10.1016/j.csda.2013.02.017
39. Mehrabian H, Myrehaug S, Soliman H et al (2018) Quantitative magnetization transfer in monitoring glioblastoma (GBM) response to therapy. Sci Rep 8:1–11. https://doi.org/10.1038/s41598-018-20624-6
40. Mehrabian H, Lam WW, Myrehaug S et al (2018) Glioblastoma (GBM) effects on quantitative MRI of contralateral normal appearing white matter. J Neurooncol 139:97–106. https://doi.org/10.1007/s11060-018-2846-0
41. Tozer DJ, Rees JH, Benton CE et al (2011) Quantitative magnetisation transfer imaging in glioma: preliminary results. NMR Biomed 24:492–498. https://doi.org/10.1002/nbm.1614
42. Garcia M, Gloor M, Bieri O et al (2015) Imaging of primary brain tumors and metastases with fast quantitative 3-dimensional magnetization transfer. J Neuroimaging 25:1007–1014. https://doi.org/10.1111/jon.12222
43. Jones CK, Huang A, Xu J et al (2013) Nuclear Overhauser enhancement (NOE) imaging in the human brain at 7T. Neuroimage. https://doi.org/10.1016/j.neuroimage.2013.03.047
44. Ray KJ, Simard MA, Larkin JR et al (2019) Tumor pH and protein concentration contribute to the signal of amide proton transfer magnetic resonance imaging. Cancer Res 79:1343–1352. https://doi.org/10.1158/0008-5472.CAN-18-2168
45. Lescher S, Jurcoane A, Veit A et al (2014) Quantitative T1 and T2 mapping in recurrent glioblastomas under bevacizumab: earlier detection of tumor progression compared to conventional MRI. Neuroradiology 57:11–20. https://doi.org/10.1007/s00234-014-1445-9
46. Müller A, Jurcoane A, Kebir S et al (2017) Quantitative T1-mapping detects cloudy-enhancing tumor compartments predicting outcome of patients with glioblastoma. Cancer Med 6:89–99. https://doi.org/10.1002/cam4.966
47. Zhang X-Y, Wang F, Li H et al (2017) Accuracy in the quantification of chemical exchange saturation transfer (CEST) and relayed nuclear Overhauser enhancement (rNOE) saturation transfer effects. NMR Biomed 30:e3716. https://doi.org/10.1002/nbm.3716
48. Bradley WG (1993) MR appearance of hemorrhage in the brain. Radiology 189:15–26. https://doi.org/10.1148/radiology.189.1.8372185
49. Kerkmeijer LGW, Fuller CD, Verkooijen HM et al (2016) The MRI-linear accelerator consortium: evidence-based clinical introduction of an innovation in radiation oncology connecting researchers, methodology, data collection, quality assurance, and technical development. Front Oncol 6:1–6. https://doi.org/10.3389/fonc.2016.00215
50. Ellingson BM, Wen PY, Cloughesy TF (2017) Modified criteria for radiographic response assessment in glioblastoma clinical trials. Neurotherapeutics 14:307–320. https://doi.org/10.1007/s13311-016-0507-6
51. Tseng C-L, Stewart J, Whitfield G et al (2020) Glioma consensus contouring recommendations from a MR-Linac International Consortium Research Group and evaluation of a CT-MRI and MRI-only workflow. J Neurooncol. https://doi.org/10.1007/s11060-020-03605-6